Evaluation of SMAP/Sentinel 1 High-Resolution Soil Moisture Data to Detect Irrigation Over Agricultural Domain

Ehsan Jalilvand, Ronnie Abolafia-Rosenzweig, Masoud Tajrishy, and Narendra N. Das

***Abstract*—Irrigation is not well represented in land surface, hydrological, and climate models. One way to account for irrigation is by assimilating satellite soil moisture data that contains irrigation signal with land surface models. In this study, the irrigation detection ability of SMAP enhanced 9 km and SMAP-Sentinel 1 (SMAP-S1), 3 km and 1 km soil moisture products are evaluated using the first moment (mean) and the second moment (variability) of soil moisture data. The SMAP enhanced 9 km soil moisture product lacks irrigation signals in an irrigated plain south of Urmia Lake, whereas SMAP-S1 products record irrigation signal in soil moisture variability. Despite observing higher variability over irrigated areas, there are only small and inconsistent wet biases observed over irrigated pixels relative to nearby nonirrigated pixels during the irrigation season. This is partly attributable to the climatology vegetation water content used in the SMAP-S1 soil moisture retrieval algorithm that is not accounting for crop rotation and land management. Thus, in the second part of this study, we updated the retrieval algorithm to use dynamic vegetation water content. The update increased vegetation water content up to 1 kg/m^2 which corresponds with a 0.05 cm^3/cm^3 increase in soil moisture during irrigation season. The update does not notably change soil moisture retrievals off season. This study shows that irrigation signals are present in both the first and second moment of soil moisture time series, and employing dynamic vegetation water content in the SMAP-S1 algorithm can enhance the irrigation signal over agricultural regions.**

***Index Terms*—Irrigation, SMAP-Sentinel 1 (SMAP-S1), soil moisture (SM), vegetation water content (VWC).**

I. Introduction

IRRIGATION is the largest human intervention in the water cycle, accounting for 70% of global freshwater withdrawals [1] that deplete groundwater reservoirs [2]–[4] while altering the terrestrial water and energy budgets [5], [6]. Studies have shown irrigation's impact on local climates, such as evaporative cooling and increasing precipitation downwind of an intensely irrigated (IR) area [7], may modulate climatological extremes and affect agricultural yields [8]. For example, Thiery *et al.* [9] pose that irrigation has dampened the impact of rising temperatures associated with global warming for nearly 1 billion people. The expected expansion of IR cropland area to meet the demands of a growing population [10], [11] underscores the necessity to include irrigation in climate and land surface models (LSMs). However, irrigation has been poorly represented in models [12] because parametrization of irrigation requires ancillary data—irrigation method, land use/cover, irrigation timing and frequency, and crop phenology—which is difficult to estimate [8]. Another way to include irrigation in modeling is to assimilate soil moisture (SM) data that contains irrigation signal [12]–[14]. Microwave observations from satellites have provided a unique tool to monitor SM on a global scale and have been shown to detect the bulk of irrigation signature over heavily IR areas such as California's Central Valley, where irrigation can be applied continuously over large areas [12]. However, the coarse resolution of microwave satellite data (>25 km) has made it difficult to resolve irrigation at small agricultural practices where irrigation is applied periodically (a common practice in most of the IR cropland around the world) [15]–[18]. In other words, the footprint of irrigation application is often smaller than microwave SM resolution.

The 1 km and 3 km SMAP-Sentinel 1 (SMAP-S1) SM data product [19] provides a unique opportunity to evaluate the detection of irrigation signal over much smaller agricultural practices. This product has a lower temporal resolution (6–12 days dependent on geographical location) compared to the SMAP gridded 9–36 km products (2–3 days) due to the narrower swath width of Sentinel 1 [19]. The frequency of SM observations is a limiting factor in studies that use the water balance of the surface soil layer to quantify irrigation water use [17]. However, when SM observations are assimilated with an LSM in a batch (using a smoother data assimilation scheme), even a nine-day gap between observations can result in a correlation larger than 0.85 relative to a known amount of irrigation [14]. Thus, the SMAP-S1 6- to 12-day return period is not a limiting factor for quantifying irrigation magnitude through SM data assimilation.

Manuscript received April 27, 2021; revised July 3, 2021; accepted October 1, 2021. Date of publication October 11, 2021; date of current version November 2, 2021. This work was supported in part by the Urmia Lake Restoration Program (ULRP) and in part by the NASA SMAP Mission Science team under Grant 80NSSC21K0907 and the NISAR Mission Science Team under Grant 80NSSC21K1181. *(Corresponding author: Narendra N. Das.)*

Ehsan Jalilvand is with the Sharif University of Technology, Tehran 11365-11155, Iran, and also with the Department of Biosystem and Agricultural Engineering, Michigan State University, Michigan, MI 48824 USA (e-mail: ehsan.jalilvand@sharif.edu).

Ronnie Abolafia-Rosenzweig is with the Research Applications Laboratory, National Center for Atmospheric Research, Boulder, CO 80301 USA (e-mail: abolafia@ucar.edu).

Masoud Tajrishy is with the Department of Civil and Environmental Engineering, Sharif University of Technology, Tehran 11365-11155, Iran (e-mail: tajrishy@sharif.edu).

Narendra N. Das is with the Department of Biosystem and Agricultural Engineering, Department of Civil and Environmental Engineering, Michigan State University, Michigan, MI 48824 USA (e-mail: dasnaren@msu.edu).

Digital Object Identifier 10.1109/JSTARS.2021.3119228

A potential limiting factor of the SMAP-S1 SM product is the lower accuracy over cropland areas (ubRMSE $= 0.07$ cm^3/cm^3) that is partly attributable to the ancillary data used in the SM retrieval algorithm [19]. One of the major updates in version 3 of SMAP-S1 1 km SM product (the most recent version at the time of this study) was replacing the Harmonized World Soil Database at $\sim$10–25 km resolution with a finer resolution soil texture map (i.e., 250 m) from the global high-resolution soil database [20]. This update significantly changed the clay fraction and, consequently, SM retrievals in most parts of the world. United States and Australia are exceptions as high-resolution clay fraction data were already employed in the SMAP-S1 SM retrieval algorithm over these countries.

Another potential source of error produced from ancillary data used to calculate SMAP-S1 SM retrievals is that the product uses vegetation water content (VWC) climatology, derived from a 10-year (2002–2012) daily average based on Moderate Resolution Imaging Spectradiometer (MODIS) observed Normalized Difference Vegetation Index (NDVI) [19]. Climatology VWC used in the SMAP-S1 algorithm is suitable for most landcover classes (93% of Earth's land surface) [19], but human impacts on landcover, e.g., irrigation, can substantially change seasonal vegetation over cropland areas that account for 7% of Earth's land area [21], [22]. Das *et al.* [19] showed that while observed (i.e., dynamic) VWC over the shrubland area remains almost similar to the climatology VWC, there is a mismatch between climatology and dynamic VWC over cropland areas due to crop rotation and land management. Higher ubRMSE of the SMAP-S1 SM product over cropland areas are partly attributed to this issue [19].

This study evaluates the SMAP-S1 1 km SM product over an IR region and evaluates modified SMAP-S1 SM retrievals that use dynamic VWC in the retrieval algorithm. This study is motivated to support future developments in the SMAP-S1 product and inform studies that rely on irrigation signals in remotely sensed SM data (e.g., [14], [16], [17]). The main objectives of this study are as follows:

1) investigate the impact of SMAP products' spatial resolution on irrigation detection (Sections III-A, IV-A, and IV-B);
2) evaluate the ability of the SMAP-S1 1 km SM product to detect irrigation signals (Sections III-B and IV-C); and
3) quantify impacts of using dynamic VWC, instead of VWC climatology, over IR and non-IR regions during irrigation and rainy seasons (Sections III-C and IV-D).

II. Study Area and Data

A. Study Area

Urmia lake basin is located in northwestern Iran and has an area of 51 000 km^2. Urmia Lake, once one of the largest hypersaline lakes in the world and a vulnerable ecosystem, is located in this basin. Urmia Lake's main sources of water are precipitation and surface water. Basin average annual precipitation (1960–2010) is 296 mm/year [16], with a decreasing trend (between 9 and 20 mm/year) over the last 20 years [23]. A total of 17 main rivers are supplying nearly 3 billion cubic meters of water to the Lake annually, but the inflow to the Lake has decreased substantially. Consequently, the Lake has lost nearly 80% of its original water extent in the last two decades (see Fig. 1), attributable to climate change (a prolonged drought) and recent water resources development in the basin [24]–[26]. [24] attributed the lake shoreline retreat to human activities, including excessive Dam construction projects and intensive agricultural activities, as they did not find any significant trend in the drought pattern or substantial increase in the evaporation rate caused by climate change over the region. Addressing these issues, Urmia Lake Restoration Program suggested multiple restoration strategies, such as stopping all reservoir development projects and reducing irrigation water use in the region by 40% in a ten-year timeframe. However, a more recent study showed that projected climate change would in fact, reduce the water availability in the basin by 10–27% in the next 40 years [25]. Thus, current restoration measures might be effective in the short term, but in the long term, they would be insufficient to maintain Lake Urmia as a robust reservoir. The role of climate change in Lake shrinkage is further emphasized in [26], who suggests that a substantial reduction (close to 50%) in agricultural water demand (as the primary consumer of freshwater in the basin) is needed to buffer the impact of climate change on the Lake, as, under current climatic conditions, surface and groundwater withdrawal for agricultural demand is comparable to (or even larger) than all other surface inflow to the Lake [26]. Indeed, the IR agriculture, which is dominated by flood irrigation with efficiency lower than 40%, has tripled in area in the last 40 years [25], and is in direct competition with the Lake as they are formed around all tributaries to the Lake and withdraw water before it reaches the Lake.

In this study, three major IR agricultural plains south of Lake Urmia, namely Miandoab, Mahabad, and Naghadeh, are considered (see Fig. 2). Water from the Zarrineh, Simineh, Mahabad, and Gadar chay rivers (collectively 60% of total lake inflow) passes through these plains. A total of 35 different crops dominated by wheat, tomatoes, potatoes, barley, sugar beets, alfalfa, and apples are cultivated in these plains [see Fig. 6(b)]. Most of the region's crops are irrigated between May to October [27] when the rainfall is negligible, and SM wetting can be attributed to irrigation; therefore, this period is chosen as the irrigation season in this study.

B. Remotely Sensed SM

We use version 4 of SMAP Enhanced 9 km (SMAP 9 km) ([28],[1]) and version 3 of SMAP-S1 3 km and 1 km SM products ([29],[2]). The SMAP 9 km product is shown to have enhanced spatial details in SM observations compared to the 36 km radiometer-based product while maintaining the mission accuracy goal of ubRMSE less than or equal to 0.04 cm^3/cm^3 [30]. Additionally, Lawston *et al.* [12] showed that an SMAP 9 km product has the ability to detect irrigation signals over heavily IR regions. Leveraging SAR high-resolution measurements,

[1][Online]. Available: https://nsidc.org/data/SPL3SMP_E
[2][Online]. Available: https://nsidc.org/data/SPL2SMAP_S

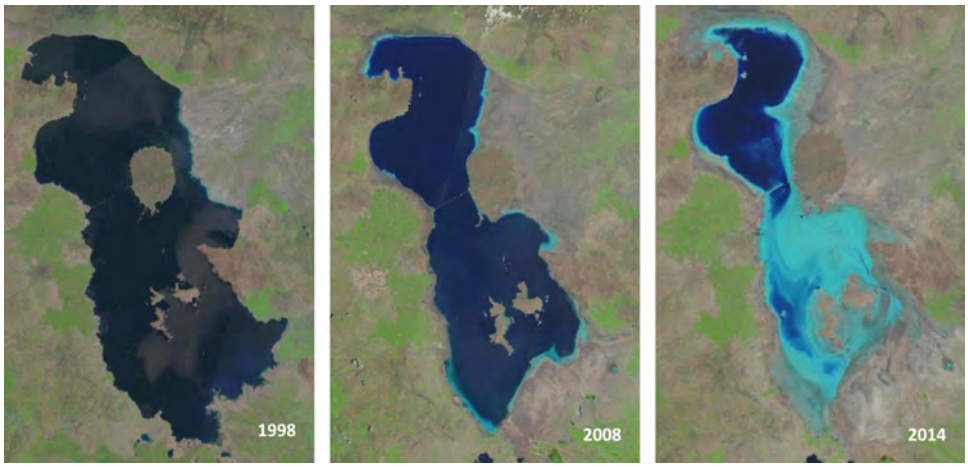

Fig. 1. Urmia lake surface water extent decline in the last two decades. *Source*: Images are from a Landsat collection available at https://landsatlook.usgs.gov.

Fig. 2. Overview of the study area, major IR cropland areas south of Urmia lake are outlined in yellow polygons.

SMAP-S1 3 km and 1 km products showed even more detailed spatial information content compared to an SMAP 9 km product at the cost of slightly lower accuracy (ubRMSE $= 0.05$) and longer return intervals (6–12 days). Both of which are associated with integrating Sentinel 1 measurement [19]. SMAP-S1 combines passive microwave measurements from the SMAP *L*-band radiometer with active *C*-band radar measurements from Sentinel 1 (A and B). A recent study by [31] shows that using *C*-band radar measurements from Sentinel 1 in place of the original SMAP *L*-band radar would increase the SM retrieval error by 0.01 cm^3/cm^3, other differences between the *C*- and *L*-band measurements such as the penetration depth and different sensitivities to land cover heterogeneity and vegetation might impact the retrieval as well. All of these updates raise the question of whether this product is better equipped to detect irrigation signal. We evaluated the ability of three SMAP products, namely SMAP 9 km, and SMAP-S1 3 km and 1 km products.

We choose to exclusively use AM overpasses from the SMAP 9 km product as it is reported to have higher quality [32]; however, in the SMAP-S1 3 km and 1 km SM products, we used both AM and PM retrievals to maximize the number of SM measurements. We further filtered the retrievals based on the difference in time of acquisition to be less than 12 h and only chose products that merge Sentinel 1 AM overpasses with either same day morning SMAP crossing or the previous day afternoon crossing to ensure the stability of SM content between the consecutive SMAP and Sentinel 1 retrievals.

1) SMAP-S1 SM Retrieval Algorithm: An active-passive algorithm was developed to estimate SM based on SMAP radar and radiometer retrievals. After the SMAP radar operation ended, the team decided to replace the Sentinel 1 SAR system to recover the high-resolution capability of the SMAP mission. Sentinel 1 has a similar orbit to SMAP, which has led to small acquisition time differences with SMAP in the overlapping swath. It also has global coverage and provides both copol and cross-pol backscattering needed for the active-passive algorithm. The main limitation is the narrower swath width of Sentinel 1 that decreases the temporal resolution from 1–3 days to 6–12 days.

The active-passive algorithm disaggregates radiometer brightness temperature (TB) using Sentinel 1 SAR data and the radiative transfer zero-order Tau–Omega model to retrieve high-resolution SM from disaggregated TB [33].

C. Precipitation

This study uses precipitation data from the Integrated Multi-satellitE Retrievals for GPM (IMERG) 0.1-degree final run V06 product ([34],[3]). Precipitation data are spatially interpolated to remotely sensed SM grids using the nearest neighbor approach.

D. NDVI and VWC

SMAP-S1 uses a ten-year climatology (2002–2012) NDVI from MODIS to estimate the VWC based on equation (1)

$$\mathrm{VWC} = 1.9134 \times \mathrm{NDVI}^2 - 0.3215 \times \mathrm{NDVI} + \mathrm{stem\ Factor} \times (\mathrm{NDVI}_{\max} - \mathrm{NDVI}_{\min}) / (1 - \mathrm{NDVI}_{\min}). \quad (1)$$

[3][Online]. Available: https://disc.gsfc.nasa.gov/datasets/GPM_3IMERGDF_06/summary

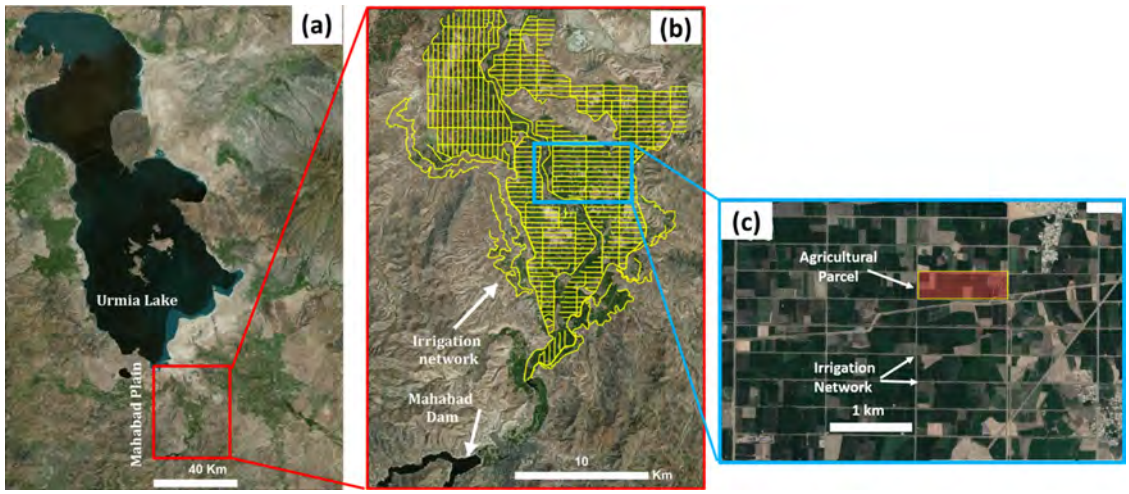

Fig. 3. Mahabad plain IR agriculture, (a) Mahabad Plain, (b) Mahabad irrigation network and the location of Mahabad dam, and (c) closer look at the agricultural parcels and irrigation canals.

TABLE I
SMAP-S1 SM RETRIEVAL CONFIGURATIONS

Name	Vegetation Water Content
Original SMAP-S1	Climatology
SMAP-S1 (dyn VWC)	Dynamic/observed

In this equation, NDVI is the NDVI retrieval from MODIS (MOD13A2 v006; [35];[4]), $\mathrm{NDVI}_{\max}$ is the annual maximum NDVI at each pixel (over cropland and grassland area the actual NDVI must be used in place of $\mathrm{NDVI}_{\max}$). $\mathrm{NDVI}_{\min}$ is the minimum annual NDVI (set to 0.1), and the stem factor depends on the land cover type (e.g., for cropland $= 3.5$ and for grassland $= 1.5$). In this study, NDVI values from MODIS are linearly interpolated in space and time to obtain NDVI used to estimate dynamic VWC based on (1) to create a modified SMAP-S1 product (dyn VWC) from Table I.

E. In Situ *Irrigation Data*

Among the three IR plains encompassed in the study area, only the Mahabad plain has a completed irrigation network [see Fig. 3(b)] and daily irrigation data for the period of the study. Daily water release records from the Mahabad dam to the Mahabad irrigation network for agricultural demand from 2017–2019 are used in this study. Due to the lack of information regarding the irrigation application heterogeneity (which motivates this study), we assume that the irrigation is applied uniformly. Thus, the volumetric water withdrawal is translated to irrigation depth by dividing it to the plain cropland area (202 km^2).

III. METHODOLOGY

We consider that irrigation signal is contained in both the first moment (mean) and second moment (variability) of the SM time series because irrigation wetting can increase both the mean and variability of SM. The ability of SMAP SM products to detect irrigation temporally is assessed in time series analyses over IR and nonirrigated (nIR) pixels during and outside of the irrigation season. We assess the ability of SMAP products to detect spatial irrigation signatures by comparing variability, quantified using the mean absolute deviation (MAD) metric, of SM during and outside of the irrigation season. A distinctly higher MAD value over the IR area during the irrigation season and nearly uniform MAD outside of irrigation season is an indicator of the irrigation mapping ability of SMAP SM product.

In the second part of this article, following [19] suggestion, we replace climatology VWC with dynamic VWC to determine if this update improves the product's ability to detect irrigation signals.

A. *Intercomparison of Different SMAP SM Products Ability to Detect Irrigation Signals*

The impact of enhanced SM spatial resolution on irrigation detection is investigated by comparing SM time series from SMAP 9 km with time series from SMAP-S1 3 km and 1 km pixels bounded within the 9 km pixel. Higher SM values and variability at finer spatial resolutions during the irrigation season are considered indicators of capturing plot scale irrigation at finer resolutions.

B. *Evaluating the Ability of the SMAP-S1 1 km Product to Detect Irrigation Signal*

The SMAP-S1 1 km SM product is better equipped to detect spatial details and SM patterns relative to SMAP 9 km; however, increasing spatial resolution adds noise associated with SAR measurements [19]. We evaluate temporal irrigation signals from the SMAP-S1 1 km product using the same approach mentioned in Section III-A. To isolate the irrigation-driven SM variation, IR and nIR pixels are chosen such that all other

[4][Online]. Available: https://lpdaacsvc.cr.usgs.gov/appeears/

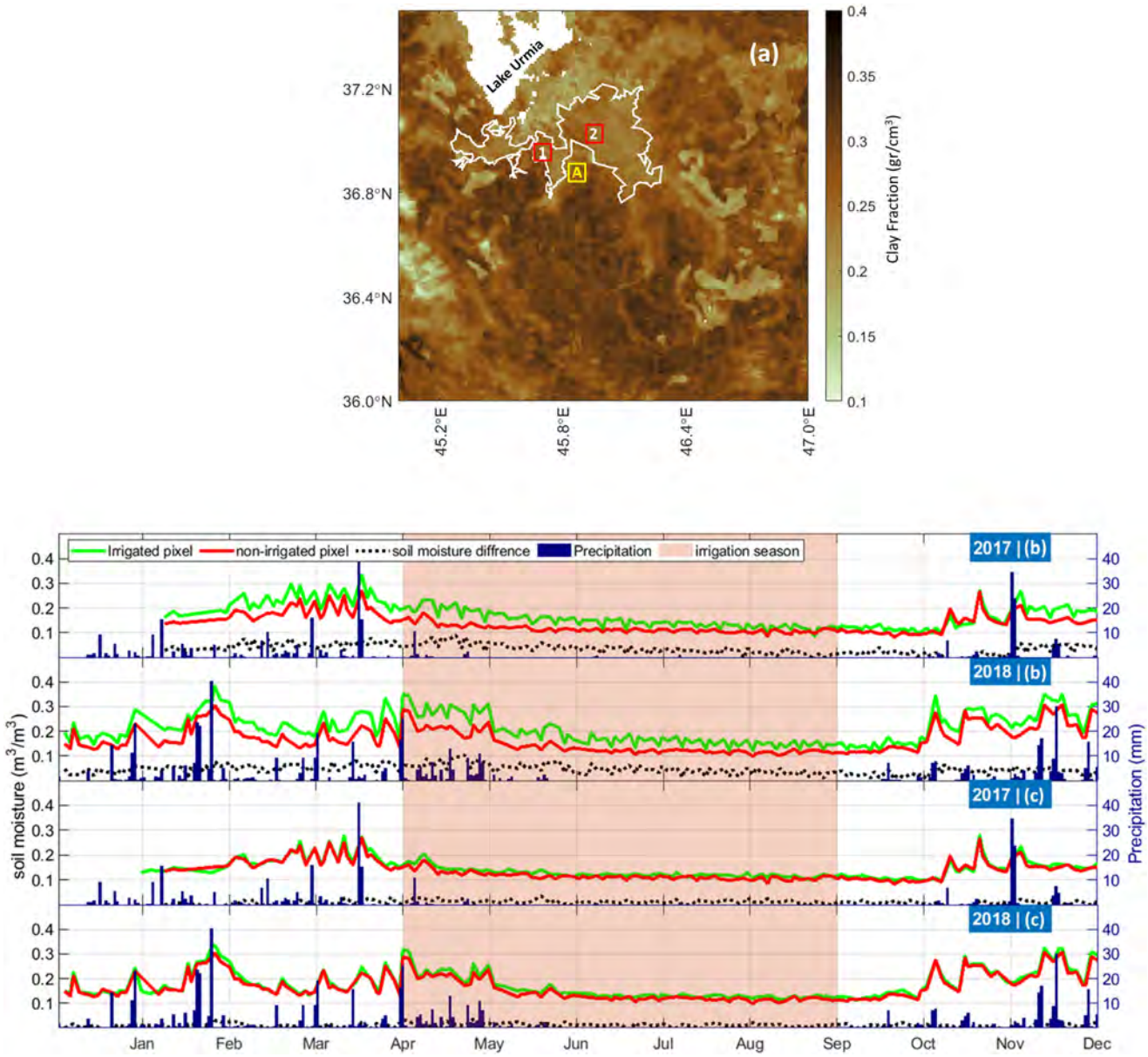

Fig. 4. 9 km SMAP product fails to resolve irrigation signal over small-scale agricultural area. (a) Location of IR and nIR pixels on the clay fraction map, (b) SMAP SM time series from an IR (1) and an nIR pixel (A), and (c) SMAP SM time series from another IR (2) and the same nIR pixel (A) from 2017 to 2019. The persistent shift between the IR and nIR time series throughout the year is illustrated as the difference between IR and nIR pixels (dashed black line). Precipitation is illustrated as vertical blue lines. The irrigation season is highlighted in pink.

factors affecting SM retrievals are similar. Thereby, pixels are chosen to be in close proximity (<15 km) to minimize the spatial precipitation gradient, to have a similar clay fraction (based on the SMAP clay fraction layer), and be located in a flat area without complex topography and far from urban areas to reduce the noise in radar backscattering.

The ability to map irrigation with the 1 km SMAP-S1 product is evaluated using the MAD index over the study area. Higher MAD values over the IR area during the irrigation season and near-uniform MAD during the off-season is an indicator of capturing irrigation-driven SM variation by the SMAP-S1 1 km product. We attempt to isolate variability in SM retrievals attributable to irrigation rather than outside factors such as changes in lake extent and variability in Sentinel-1 backscattering. Fluctuation in the Urmia Lake extent can impose trends in SM retrievals surrounding the Lake, so we detrend retrievals using a piecewise linear technique before calculating MAD. Complex topography distorts incident angles of SMAP and Sentinel 1 observations and increases uncertainties in TB and backscatter data, respectively. Thus, we mask the study area based on the standard deviation of slope within each SMAP-S1 1 km grid cell to only consider relatively flat pixels (with slope standard deviation lower than 6% as used in the SMAP SM processing, [33]) in this analysis.

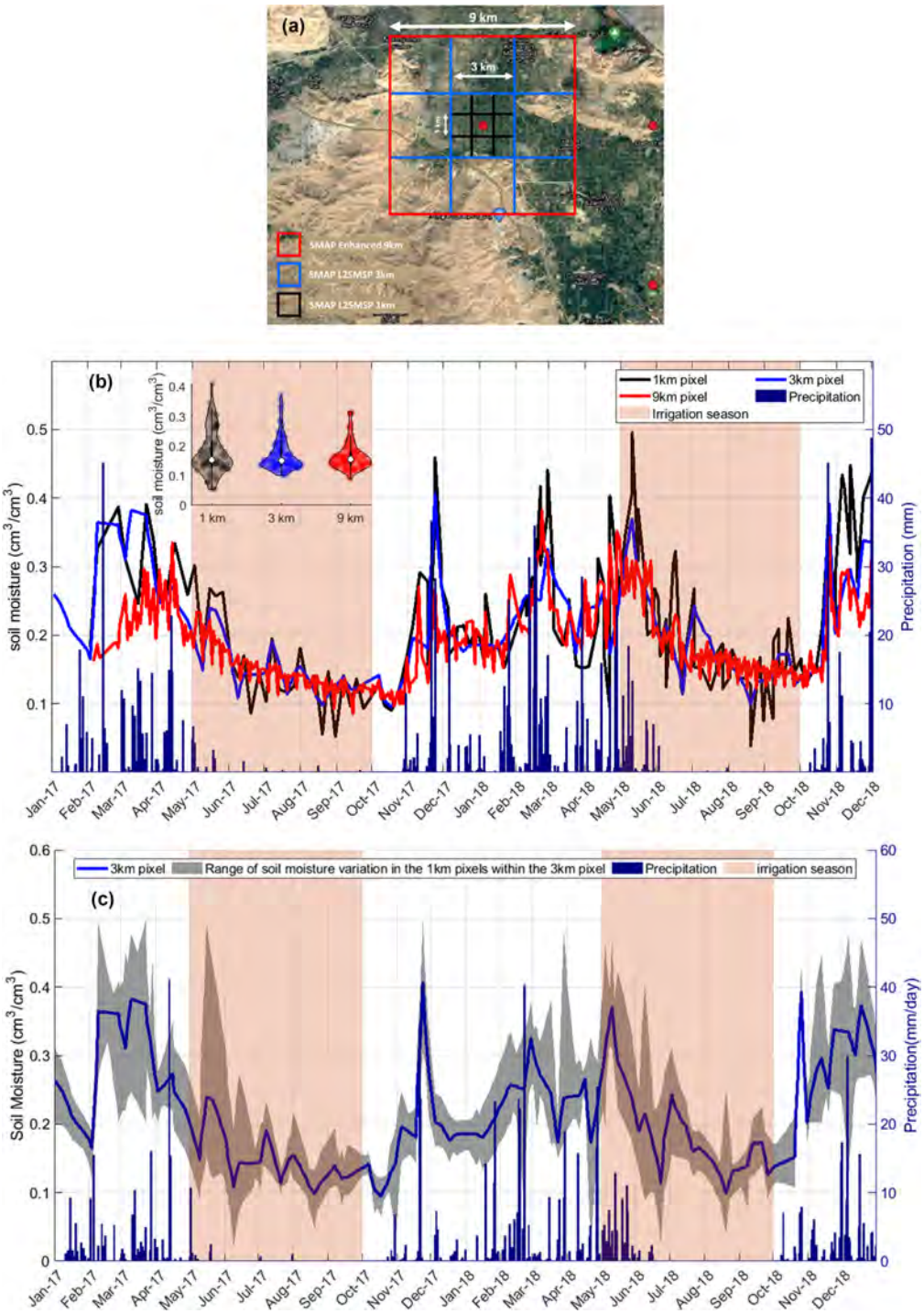

Fig. 5. SM heterogeneity in SMAP retrievals resolved by original SMAP-S1 1 km product. (a) SMAP EASE-Grid 2 for a 9 km (red), 3 km (blue), and 1 km (black) pixel over an agricultural region in Mahabad plain, (b) SM time series from the 9 km SMAP product (red line) with the corresponding 3 km (blue line) and 1 km (black line) pixels from the SMAP-S1 product that are located at the center of the bounding 9 km pixel (denoted by the red dot), the inset shows the violin plot of each SM timeseries during the irrigation season (c) SM time series at the center 3 km pixel (solid blue line) with the range of SM variation in the nine bounded 1 km pixels (gray shaded area).

C. Evaluating the Impact of Using Dynamic VWC on the SMAP-S1 SM Retrieval

Modifications to ancillary data in the SMAP-S1 retrieval algorithm may provide more realistic portrayals of SM over IR areas. Specifically, in this study, we run the SMAP-S1 SM retrieval algorithm by replacing climatology VWC with dynamic VWC obtained from MODIS 1 km NDVI. We evaluate changes in SM retrievals corresponding with this modification for two different configurations of SM products based on the usage of VWC input

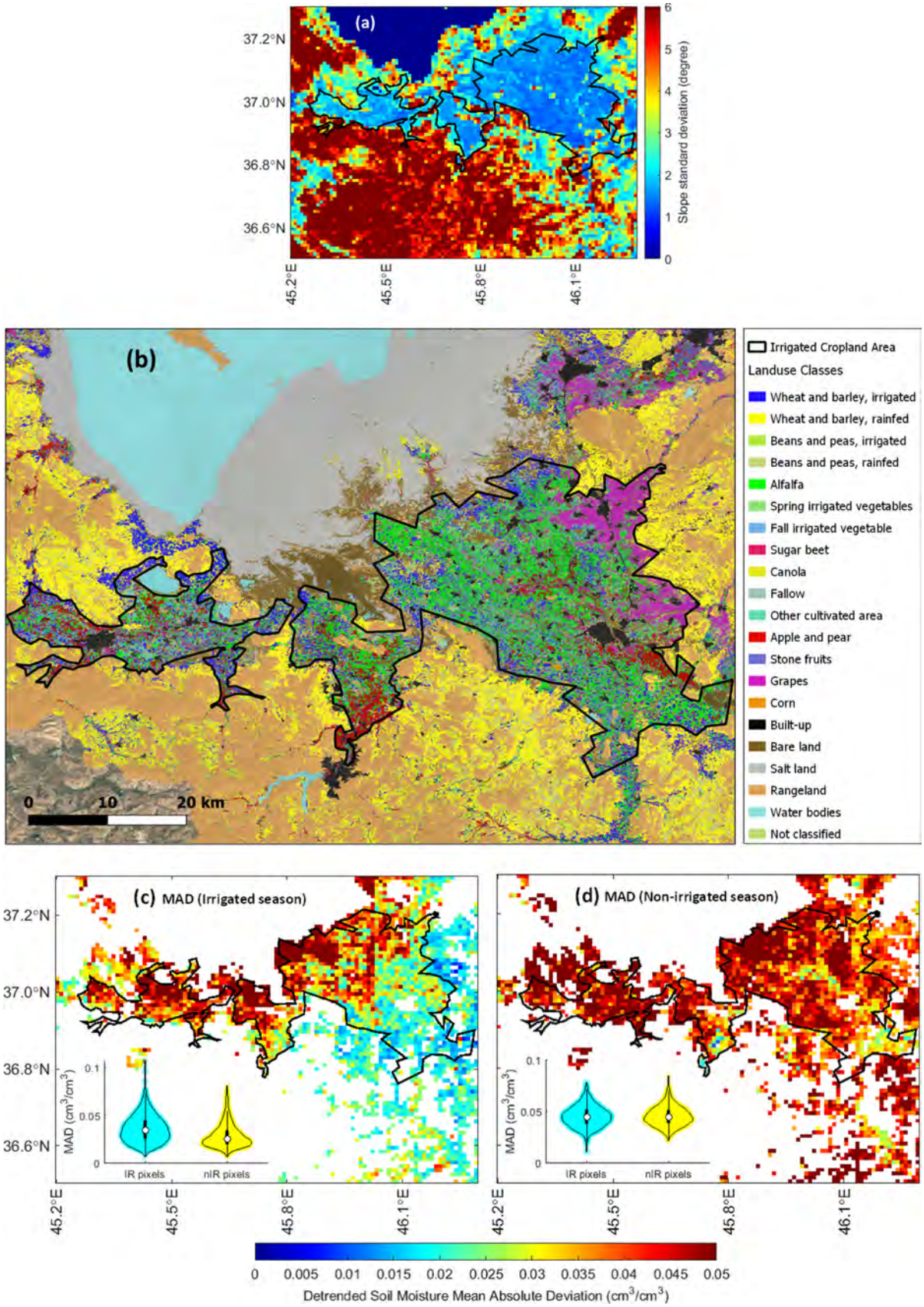

Fig. 6. Mapping IR area using SM variability (MAD), (a) slope standard deviation within each 1 km SMAP-S1 pixel which serves as the basis of screening topographically complex areas (see Section III-B), (b) crops cultivated south of Urmia Lake [41], (c) MAD of the SMAP-S1 1 km product during irrigation seasons (May–October) of 2017 and 2018, and (d) MAD of the SMAP-S1 1 km product during the off-seasons (January–April and October–December) of 2017 and 2018. Insets in (c) and (d) show violin plots of MAD over IR (cyan) and nIR areas (yellow) during the irrigation season and rainy season, respectively.

(see Table I). Increases in SM magnitude and variability during the nonrainy season over IR areas are considered enhancements in irrigation detection.

The impacts associated with the VWC update are assessed by i) comparing dynamic VWC with climatology VWC and then ii) comparing original SMAP-S1 with SMAP-S1 (dyn- VWC). The comparison is carried out temporally over an IR and an nIR pixel during the study period (2017–2019) and spatially over the study area during a heavily IR month (August 2017) and a nIR month (March 2017).

IV. Results

A. Evaluating Irrigation Signal From the SMAP 9 km SM Product

There is no coherent irrigation signal in the SM time series from the SMAP 9 km in the study area. Specifically, biases between SM from IR and nIR pixels are similar in both rainy and IR seasons (see Fig. 4). The persistent bias between SM in IR and nIR pixels [see Fig. 4(b)] is likely attributable to having different surface physical properties [see Fig. 4(a)]. Thus, it seems that the SMAP 9 km product is insensitive to small-scale irrigation practices in the region.

B. Intercomparison of Different SMAP SM Products Ability to Detect Irrigation Signals

SMAP-S1 products with higher spatial resolutions (1–3 km) record more dynamic SM [see Fig. 5(b)] relative to the 9 km SMAP product. Likewise, Fig. 5(c) shows large spatial heterogeneity even within a 3 km SMAP-S1 SM retrieval, shown by the spread of retrievals from the 1 km product within a bounding 3 km pixel. Overall, Fig. 5 suggests that the irrigation signal in the 9 km pixel is averaged out during the irrigation season, and the signal is more visible in higher resolution SM retrievals.

C. Evaluating the Ability of the SMAP-S1 1 km Product to Detect Irrigation Signal

We are able to partially map the IR cropland area south of Urmia Lake [Fig. 6(b), black polygons] by quantifying the SM dynamics of the 1 km SMAP-S1 product using MAD. Fig. 6 highlights two notable features. First, during the dry season, when croplands are irrigated, the MAD is higher within the cropland region relative to the surrounding barren landscape [see Fig. 6(c)], demonstrating that the SMAP-S1 product captures the irrigation activities. Second, there are substantially smaller differences in MAD between cropland and barren areas during rainy seasons when irrigation plays a smaller role [see Fig. 6(d)]. It should be underlined that over agricultural regions, higher MAD values are mainly observed over the crop farming area [e.g., irrigated wheat, barley, and alfalfa, see Fig. 6(b)] rather than orchard farming [e.g., apple and grapes, see Fig. 6(b)]. This can be attributed to the limited ability of *C*-band penetration in the developed tree canopy.

Fig. 7 supports results from Fig. 6, showing significantly higher variability in SM ($p < 0.01$) due to frequent SM wetting over IR pixels during the irrigation season and nearly equal variation ($p > 0.2$) in the IR and nIR pixels off-season (see Table S1 of the supplementary material for more details). Higher variability

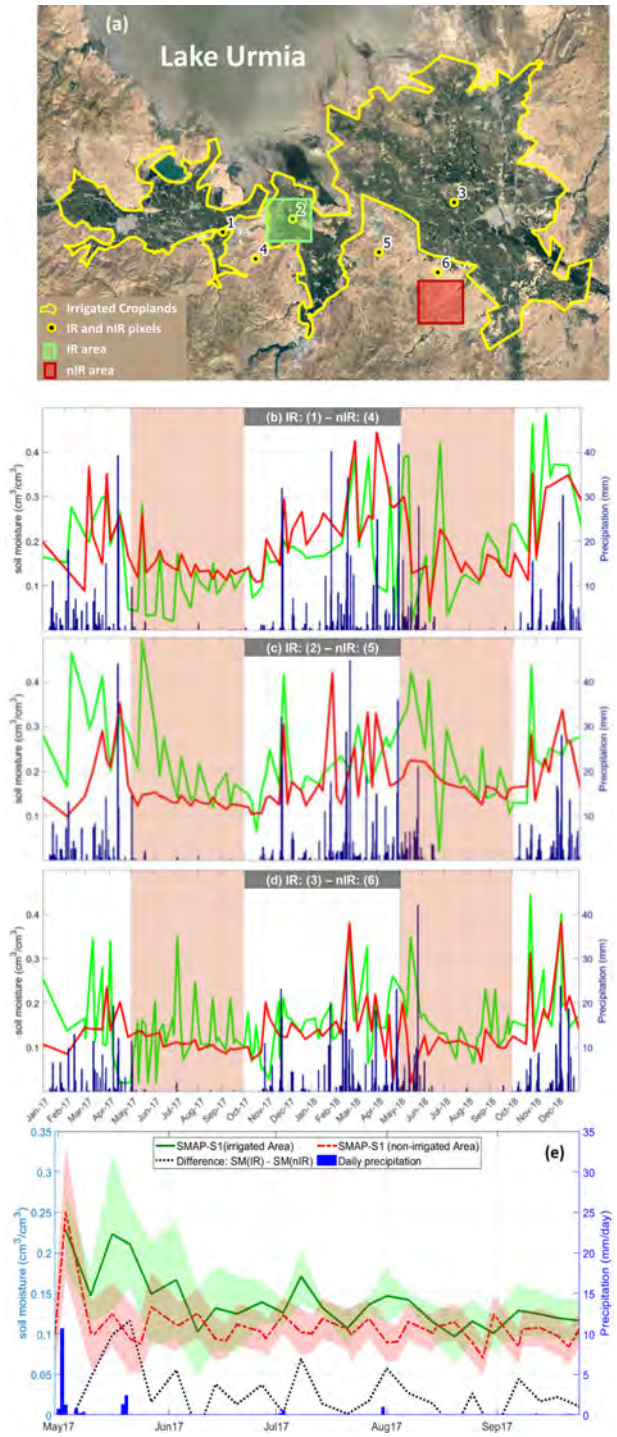

Fig. 7. Detecting irrigation signal using the SMAP-S1 1 km product in different sets of IR and nIR pixels (a) location of 1 km IR and nIR pixels, and (b)–(d) comparing SM from SMAP-S1 1 km product in six pairs of IR and nIR pixels during the irrigation season and off-season, and (e) time series of mean SM over the IR and nIR area [green and red region in (a), respectiively] during the irrigation season of 2017, with shaded area showing spatial standard deviation at each date.

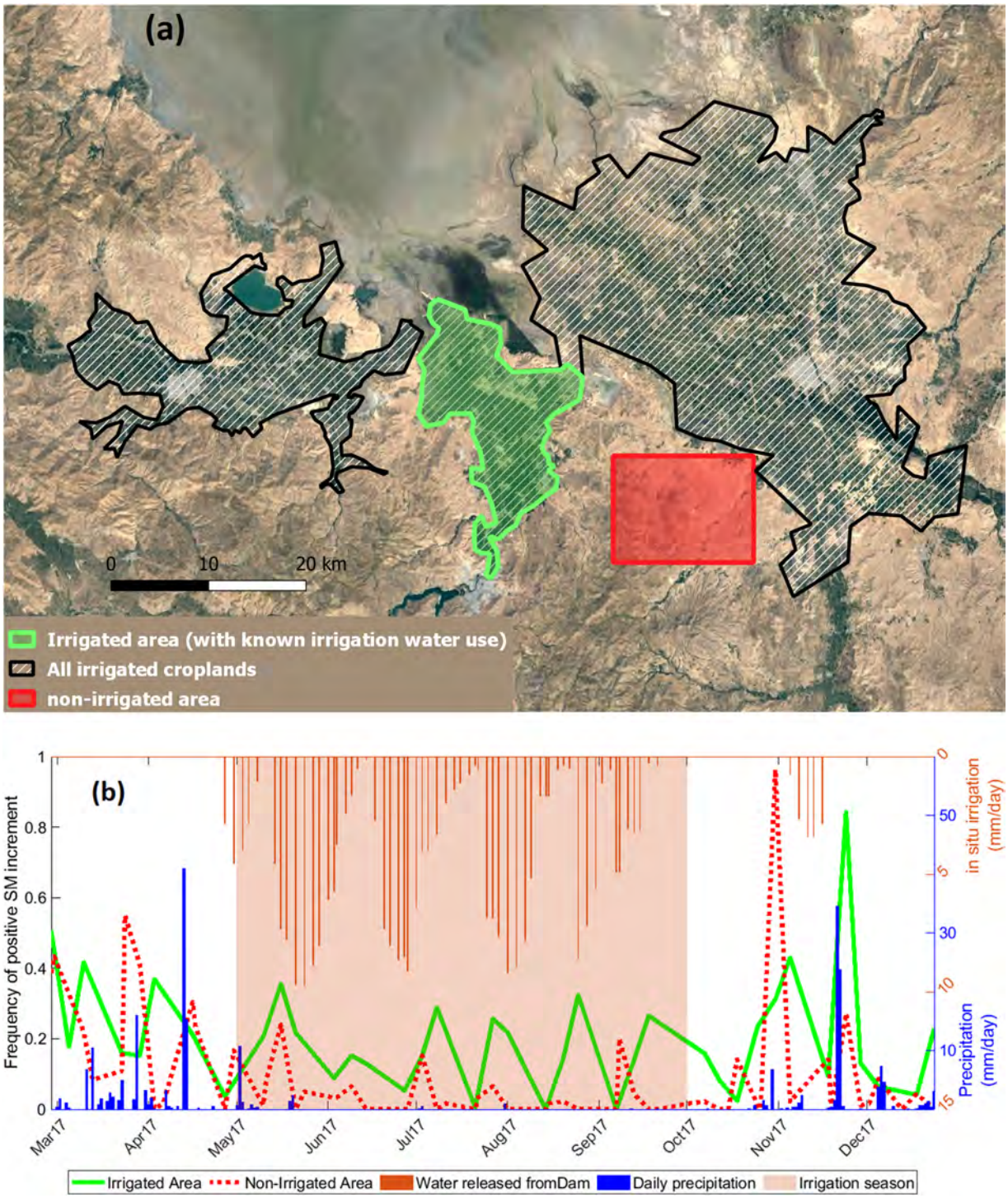

Fig. 8. Frequency of observing pixels with positive increment over IR area is higher than the nIR area during the nonrainy irrigation season. (a) Boundary of IR (green polygon) and nIR area (red recatangle) that used to calculate the fraction of pixels with positive increment, and (b) Frequency of observing positive increment in SM over IR region (green line) and nIR area (dashed red line). The blue bar plot represents precipitation, and the brown bar plots atop (b) show the water released from the Mahabad dam for agricultural demand. The pink highlighted period represents the irrigation season.

in SM is also observed in the time series of average SM [see Fig. 7(e)] over IR and nIR regions [green and red region in Fig. 7(a), respectively]. Despite consistently higher variability in the IR pixels, the mean SM state can be higher for corresponding nIR pixels [e.g., Fig. 7(b)]. This can be attributable to SMAP TB, representing an integrated value of all the fine-scale geophysical signatures within SMAP's native resolution. Hence, the overall TB is impacted by SM from cropland and barren regions within SMAP's coarse pixels, which influences the average value of SMAP TB in the active-passive disaggregation. Subsequently,

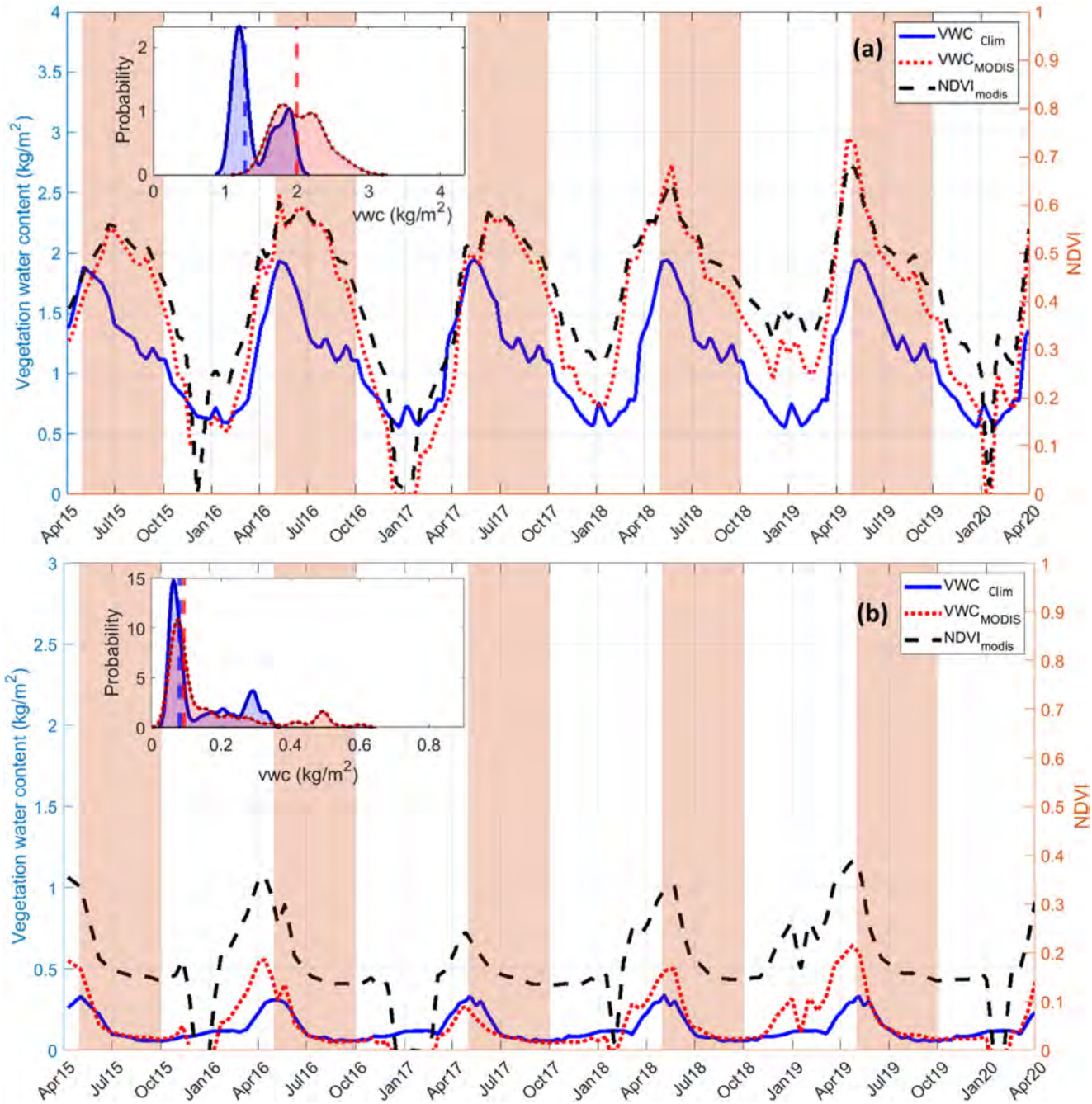

Fig. 9. Dynamic VWC shows large differences relative to climatology VWC over an IR pixel. Time series of VWC from climatology (solid blue line), MODIS-derived Actual VWC (dotted red line), and NDVI (dashed black line) in an (a) IR pixel and (b) nIR pixel. The pink highlighted periods are irrigation seasons. Insets compare the probability distribution of climatology and dynamic VWC during the irrigation season with vertical dashed lines in the insets showing mean values.

this results in similar TB being assigned to high-resolution nIR and IR pixels if there is no substantial spatial deviation in Sentinel-1 backscatter [19]. Thus, it is possible for pixel 4 to receive an irrigation signal from the two adjacent cropland regions [see Fig. 7(a)], and the irrigation signal in pixel 1 can be averaged out by the surrounding nIR pixels.

Fig. 8 shows the fraction of pixels with a positive increment in SM (larger than SMAP-S1 ubRMSE $= 0.05$ cm3/cm3) over the IR and nIR area at each date. The frequency of observing positive increments over the IR region during the irrigation season is higher than the nIR region. These wetting events correspond with the water released from the upstream dam. This pattern is also observed in other years (not shown). This result further confirms that the variation in SMAP-S1 SM product over the IR area during the irrigation season is in response to the irrigation applications.

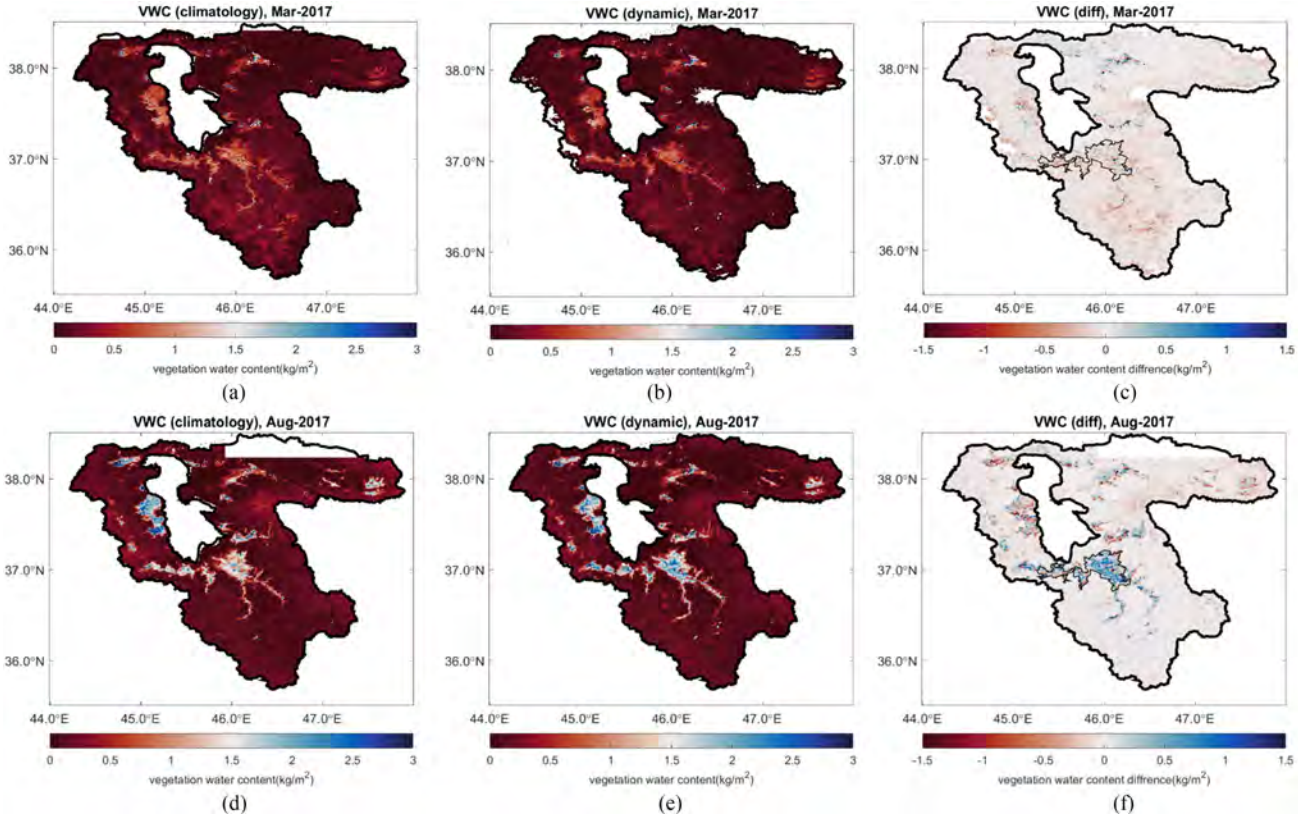

Fig. 10. Dynamic VWC shows significant differences relative to climatology VWC over an IR area during the irrigation season. The upper panel shows (a) climatology VWC, (b) MODIS-derived dynamic VWC, and (c) their difference during a rainy season (March 2017). The lower panel shows (d) climatology VWC, (e) MODIS-derived Actual VWC, and (f) their difference during an irrigation season (August 2017).

D. Impact of Using Dynamic VWC on SM Retrieval

Differences between climatology and dynamic VWC over the IR study area [see Fig. 9(a); Fig. 10(f)] cause significant differences in SM retrievals. For example, differences between climatology and dynamic VWC can reach, and even exceed, 1 $\mathrm{kg/m^2}$ which results in approximately a 0.05 $\mathrm{cm^3/cm^3}$ increase in the retrieved SM [36]. Noting that this difference in SM is significant relative to the magnitude of the irrigation signal in sandy textured soil. Dynamic and climatology VWC follow different phenology over an IR pixel, such that the probability distribution of dynamic VWC in the irrigated cropland region is distinctly bimodal with 0.7 $\mathrm{kg/m^2}$ higher mean VWC relative to the climatology VWC [see Fig. 9(a), inset). These differences may be attributable to interannual changes in irrigation practices and crop rotation [19]. Figs. 9(b) and 10(c) support that climatological and dynamic VWC yield similar results outside of IR areas in the study domain.

SM calculated with dynamic VWC is significantly and consistently higher ($p < 0.001$) than SM calculated with climatology VWC over the example pixel [see pixels 2 in Fig. 7(a)] represented in Fig. 11; note that these differences are exclusive to IR areas during the irrigation season. Large precipitation events [e.g., March 2018 in Fig. 11(a)] can have acute effects on VWC and cause deviations from climatology VWC, but distinct from irrigation seasons, these differences are not persistent. Using dynamic VWC during the irrigation season tripled the number of dates with higher SM in the IR pixel (97% of the time) relative to the nIR pixel (30% of the time). Note that differences between dynamic and climatology VWC are relatively small at all times at the chosen nIR pixel [see Fig. 11(b)].

Fig. 12 highlights the spatial consistency of results from Fig. 11, showing that irrigation can be mapped using the difference in the mean SM from dynamic and climatology VWC. The mean SM state of retrievals calculated using dynamic VWC is significantly higher ($p < 0.001$) during the growing season such that higher SM over 65% of the irrigated cropland area are obtained, while it does not show a noticeable pattern during the off-season (see Fig. 12). However, changing from climatology to dynamic VWC does not significantly improve the SMAP-S1 irrigation mapping ability using MAD (not shown). Overall, these results support that using dynamic VWC will enhance remotely sensed SM irrigation signatures.

V. Discussion

A. Investigating Different Factors Affecting Detection of Irrigation Signature by Satellite SM Data

1) Spatial Resolution: SMAP 9 km SM shows no distinct wet bias during the irrigation season over IR pixels relative to nIR pixels. However, a higher magnitude and variation of SM is

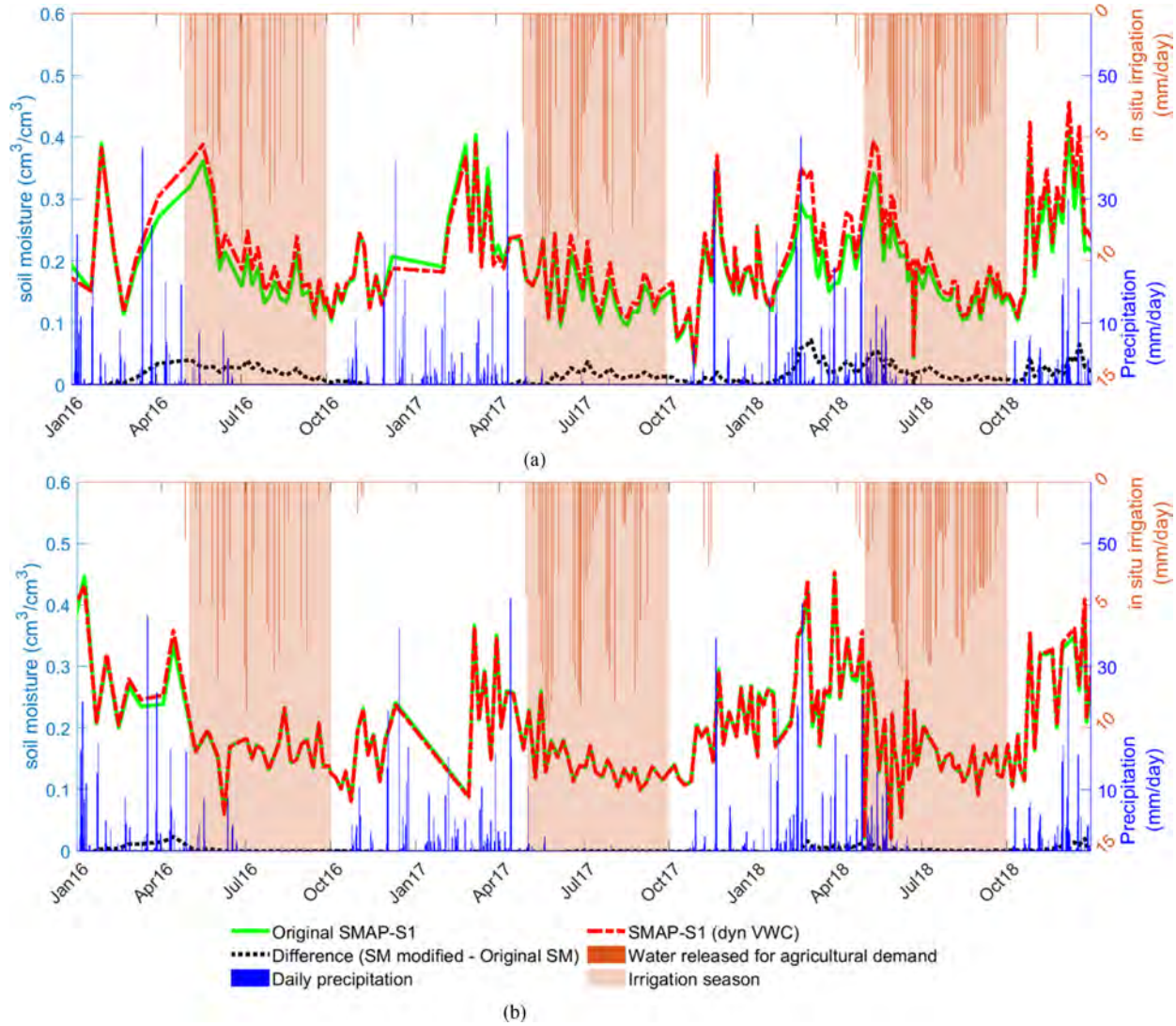

Fig. 11. Using dynamic VWC corresponds with increases in SM in the IR pixels during the irrigation season, while having almost no impact during the rainy season and in the nIR pixels. (a) Time series of original SMAP-S1 SM data (the solid green line) and the modified SMAP-S1 product [SMAP-S1 (dyn VWC), the dashed red line] over an IR and (b) nIR pixel. The black dotted line shows the difference between the Original SMAP-S1 and SMAP-S1 (dyn VWC). The blue bar plot represents precipitation, and the brown bar plots atop (a) and (b) show the water released from the Mahabad dam for agricultural demand. The pink highlighted period represents the irrigation season.

observed in the 3 km and 1 km SMAP-S1 SM products. These results are consistent with those of [12], who showed SMAP SM only contains irrigation signatures over rice fields that were continuously flooded throughout the irrigation season; whereas differences in SMAP SM for sprinkler-based IR and nIR pixels were within the range of SMAP SM error (0.04 $\mathrm{cm}^3/\mathrm{cm}^3$). The same issue is reported in studies where coarse-scale microwave products were used to quantify irrigation [15]–[18]. Indeed, the difficulty of resolving small-scale irrigation has resulted in a systematic underestimation of irrigation water use in these studies.

2) Is SM Variation or Magnitude More Affected by Irrigation in the SMAP-S1 1 km SM Product?: Irrigation signals appear to be visible in SM variation as IR plains stand out in the MAD map [see Fig. 6(c)]. This result is also supported by [37], in which SM variation was reproduced effectively over the agricultural region using satellite SM data. However, over the majority of plot scale agriculture, no significant increase in SM (higher than 0.05 $\mathrm{cm}^3/\mathrm{cm}^3$) is observed. One plausible explanation can be a smaller footprint of irrigation compared to satellite resolution. The average size of cropland plots are about 0.5 km^2 globally, and most of the plots are formed around the rivers in narrow valleys [38]; thus, it seems that there is still room for improving SM spatial resolution for resolving small agricultural practices. Future high-resolution satellite SM missions such as the NASA-ISRO Synthetic Aperture Radar Mission (NISAR), a joint mission by NASA, and Indian space agency (ISRO) plan to be launched in 2023, with 200 m spatial resolution and global coverage every 6 days, or a merged satellite and hyper-resolution LSM SM product such as SMAP-HydroBlocks at 30 m spatial resolution [39] can potentially fill the gap for agricultural monitoring using satellite SM data.

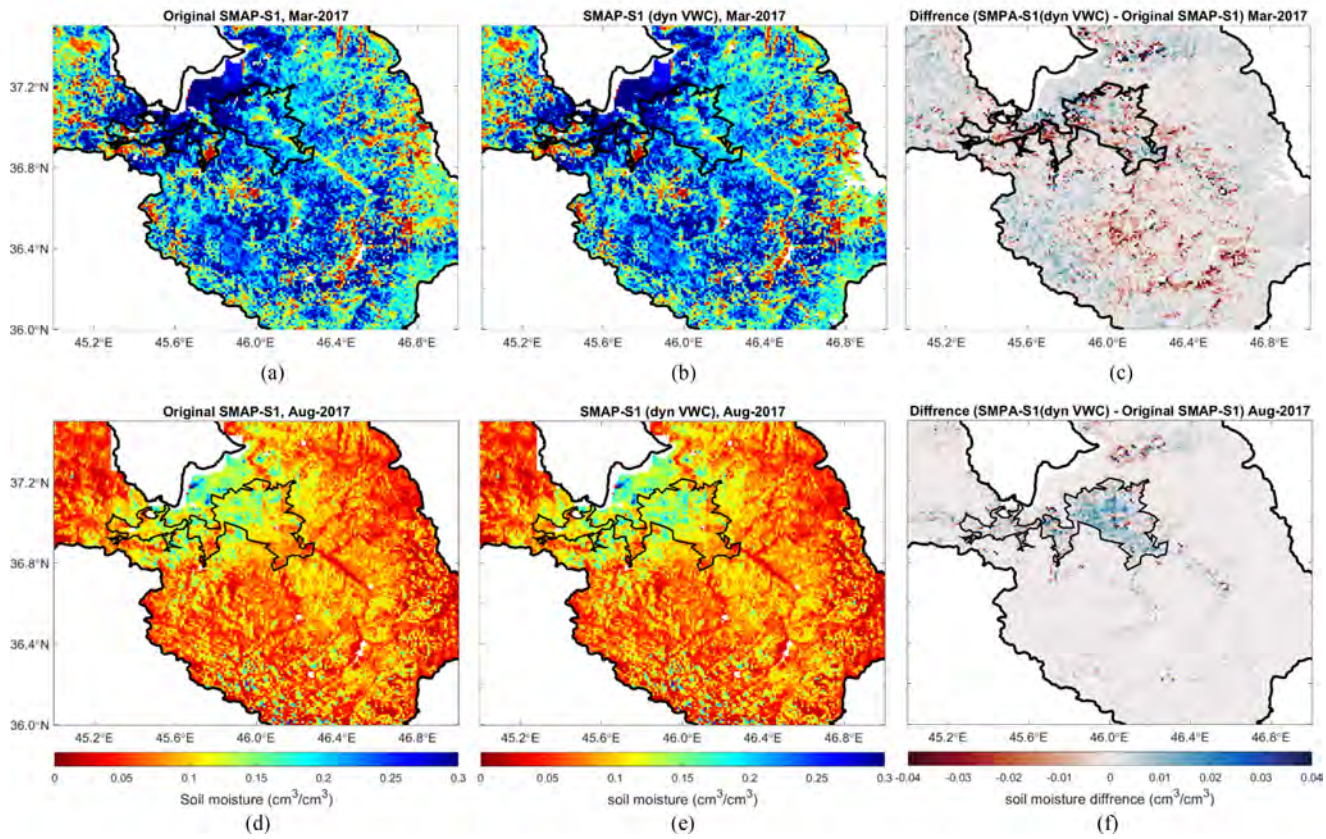

Fig. 12. SM retrievals using dynamic VWC are significantly different from retrievals using climatology VWC during the irrigation season. The upper panel shows (a) SM retrieval using climatology VWC (Original SMAP-S1), (b) SM retrieval using MODIS-derived dynamic VWC [SMAP-S1 (dyn VWC)], and (c) their difference during a rainy season (March 2017). The lower panel shows (d) SM retrieval using climatology VWC (Original SMAP-S1), (e) SM retrieval using MODIS-derived Actual VWC [SMAP-S1 (dyn VWC)], and (f) their difference during an irrigation season (August 2017).

3) Updating VWC at a Global Scale: Increases in VWC result in higher SM in the SMAP-S1 1 km product while SM MAD remains relatively unchanged. The SMAP team may plan to add dynamic VWC to improve product accuracy, especially over agricultural areas using cross-polarized backscattering from Sentinel 1 that is proportional to the vegetation density. According to the result of our study, this change is expected to enhance the irrigation signal in the first moment of the SM data during the irrigation season.

B. Assimilation of SMAP-S1 SM in LSMs

This study provides background knowledge about irrigation signatures from fine-scale remotely sensed SM that will inform an ongoing study where the modified (SMAP-S1 dyn VWC) product will be assimilated within an LSM using a particle batch smoother to estimate irrigation water use over the Mahabad Plain (see Fig. 3). Following suggestions from [14], [40], biases between modeled SM and remotely sensed SM will be removed by calibrating LSM parameters to minimize biases between simulated and SMAP-S1 (dyn VWC) SM. Therefore, this study presented herein fundamentally supports the evaluation of a new method to estimate irrigation quantities using data assimilation [14].

VI. Conclusion

This study evaluated the ability of SMAP-S1 SM products in the detection of irrigation signal over a semiarid agricultural region. The SMAP-S1 1 km product has larger SM variability relative to the 9 km SMAP and 3 km SMAP-S1 products. SMAP-S1 1 km data is able to map IR areas using the second moment of SM (MAD). This persistent higher variability is also evident in the SM time series of the IR pixels; however, the mean SM state is sometimes similar or even higher in the neighboring nIR pixels. The absence of wetting bias between IR and nIR pixels during the irrigation season might be related to the active-passive algorithm and the ancillary data used in the SMAP-S1 SM retrieval algorithm. Therefore, climatology VWC was replaced by dynamic VWC in the SMAP retrieval algorithm. Dynamic VWC modifications correspond with increases in VWC (up to 1 kg/m^2) over IR pixels during the irrigation season, while climatology and dynamic VWC are similar over nIR pixels. This, in turn, resulted in up to 0.05 cm^3/cm^3 higher estimates of SM values in the study area. These results improve the hydrologic community's fundamental understanding of irrigation signal in fine-scale remotely sensed SM and will support an ongoing study that uses data assimilation to estimate irrigation water use. Additionally, these results will aid future developments of SMAP-S1 SM products and suggest the inclusion of dynamic (i.e., observed) VWC assessed herein.

APPENDIX

A. Testing the Similarity of Variance in SM Time Series Over IR and nIR Pixels During the Irrigation and Off Season

Table S1 shows the MAD values for each IR (denoted by green) and nIR (denoted by red) pixels in Fig. 7. Moreover, a right-tale two-sample *F*-test was used to test the similarity of the variance between each pair of the IR and nIR pixels shown in Fig. 7 during the irrigation season and off season and the *p*-values are reported in Table S1. The result of *F*-test shows that the variance of IR pixels SM time series during the irrigation season is significantly larger than the nIR pixels while it is equal during the nIR season.

ACKNOWLEDGMENT

The authors would like to thank the data support from the National Snow and Ice Data Centre (NSIDC), Boulder, CO, USA, for the SMAP data products.

REFERENCES

[1] J. A. Foley *et al.*, "Solutions for a cultivated planet," *Nature*, vol. 478, no. 7369, pp. 337–342, 2011.
[2] J. S. Famiglietti *et al.*, "Satellites measure recent rates of groundwater depletion in California's central valley," *Geophys. Res. Lett.*, vol. 38, no. 3, p. L03403, 2011, doi: 10.1029/2010GL046442.
[3] M. Rodell, I. Velicogna, and J. S. Famiglietti, "Satellite-based estimates of groundwater depletion in India," *Nature*, vol. 460, no. 7258, pp. 999–1002, Aug. 2009, doi: 10.1038/nature08238.
[4] B. R. Scanlon *et al.*, "Groundwater depletion and sustainability of irrigation in the US high plains and central valley," in *Proc. Nat. Acad. Sci.*, vol. 109, no. 24, pp. 9320–9325, Jun. 2012, doi: 10.1073/pnas.1200311109.
[5] I. Haddeland, T. Skaugen, and D. P. Lettenmaier, "Hydrologic effects of land and water management in North America and Asia: 1700–1992," *Hydrol. Earth Syst. Sci.*, vol. 11, no. 2, pp. 1035–1045, Mar. 2007, doi: 10.5194/hess-11-1035-2007.
[6] M. Ozdogan, Y. Yang, G. Allez, and C. Cervantes, "Remote sensing of irrigated agriculture: Opportunities and challenges," *Remote Sens.*, vol. 2, no. 9, pp. 2274–2304, Sep. 2010, doi: 10.3390/rs2092274.
[7] A. DeAngelis, F. Dominguez, Y. Fan, A. Robock, M. D. Kustu, and D. Robinson, "Evidence of enhanced precipitation due to irrigation over the great plains of the United States," *J. Geophys. Res.*, vol. 115, no. D15, Aug. 2010, Art. no. D15115, doi: 10.1029/2010JD013892.
[8] P. M. Lawston, J. A. Santanello, B. F. Zaitchik, and M. Rodell, "Impact of irrigation methods on land surface model spinup and initialization of WRF forecasts," *J. Hydrometeorol.*, vol. 16, no. 3, pp. 1135–1154, Jun. 2015, doi: 10.1175/JHM-D-14-0203.1.
[9] W. Thiery *et al.*, "Warming of hot extremes alleviated by expanding irrigation," *Nature Commun.*, vol. 11, no. 1, Dec. 2020, Art. no. 290, doi: 10.1038/s41467-019-14075-4.
[10] D. Tilman and M. Clark, "Food, agriculture & the environment: Can we feed the world & save the Earth?," *Daedalus*, vol. 144, no. 4, pp. 8–23, Sep. 2015, doi: 10.1162/DAED_a_00350.
[11] H. C. J. Godfray *et al.*, "Food security: The challenge of feeding 9 billion people," *Science*, vol. 327, no. 5967, pp. 812–818, Feb. 2010, doi: 10.1126/science.1185383.
[12] P. M. Lawston, J. A. Santanello, and S. V. Kumar, "Irrigation signals detected from SMAP soil moisture retrievals," *Geophys. Res. Lett.*, vol. 44, no. 23, pp. 11860–11867, Dec. 2017, doi: 10.1002/2017GL075733.
[13] S. V. Kumar *et al.*, "Evaluating the utility of satellite soil moisture retrievals over irrigated areas and the ability of land data assimilation methods to correct for unmodeled processes," *Hydrol. Earth Syst. Sci.*, vol. 19, no. 11, pp. 4463–4478, 2015, doi: 10.5194/hess-19-4463-2015.
[14] R. Abolafia-Rosenzweig, B. Livneh, E. E. Small, and S. V. Kumar, "Soil moisture data assimilation to estimate irrigation water use," *J. Adv. Model. Earth Syst.*, vol. 11, no. 11, pp. 3670–3690, Nov. 2019, doi: 10.1029/2019MS001797.
[15] F. Zaussinger, W. Dorigo, A. Gruber, A. Tarpanelli, P. Filippucci, and L. Brocca, "Estimating irrigation water use over the contiguous United States by combining satellite and reanalysis soil moisture data," *Hydrol. Earth Syst. Sci.*, vol. 23, pp. 897–923, 2019, doi: 10.5194/hess-23-897-2019.
[16] E. Jalilvand, M. Tajrishy, S. A. Ghazi Zadeh Hashemi, and L. Brocca, "Quantification of irrigation water using remote sensing of soil moisture in a semi-arid region," *Remote Sens. Environ.*, vol. 231, Sep. 2019, Art. no. 111226, doi: 10.1016/j.rse.2019.111226.
[17] L. Brocca *et al.*, "How much water is used for irrigation? A new approach exploiting coarse resolution satellite soil moisture products," *Int. J. Appl. Earth Obs. Geoinf.*, vol. 73, pp. 752–766, Dec. 2018, doi: 10.1016/j.jag.2018.08.023.
[18] M. J. Escorihuela and P. Quintana-Seguí, "Comparison of remote sensing and simulated soil moisture datasets in mediterranean landscapes," *Remote Sens. Environ.*, vol. 180, pp. 99–114, 2016.
[19] N. N. Das *et al.*, "The SMAP and copernicus sentinel 1A/B microwave active-passive high resolution surface soil moisture product," *Remote Sens. Environ.*, vol. 233, 2019, Art. no. 111380, doi: 10.1016/j.rse.2019.111380.
[20] T. Hengl *et al.*, "SoilGrids250m: Global gridded soil information based on machine learning," *PLoS One*, vol. 12, no. 2, 2017, Art. no. e0169748, doi: 10.1371/journal.pone.0169748.
[21] C. J. Vörösmarty, P. Green, J. Salisbury, and R. B. Lammers, "Global water resources: Vulnerability from climate change and population growth," Science, vol. 289, no. 5477, pp. 284–288, 2000.
[22] P. Döll and S. Siebert, "Global modeling of irrigation water requirements," *Water Resour. Res.*, vol. 38, no. 4, pp. 8–10, 2002, doi: 10.1029/2001WR000355.
[23] P. Saemian, O. Elmi, B. D. Vishwakarma, M. J. Tourian, and N. Sneeuw, "Analyzing the lake Urmia restoration progress using ground-based and spaceborne observations," *Sci. Total Environ.*, vol. 739, Oct. 2020, Art. no. 139857, doi: 10.1016/j.scitotenv.2020.139857.
[24] A. AghaKouchak *et al.*, "Aral sea syndrome desiccates lake Urmia: Call for action," *J. Great Lakes Res.*, vol. 41, no. 1, pp. 307–311, Mar. 2015, doi: 10.1016/j.jglr.2014.12.007.
[25] S. Shadkam, F. Ludwig, P. van Oel, Ç. Kirmit, and P. Kabat, "Impacts of climate change and water resources development on the declining inflow into Iran's Urmia lake," *J. Great Lakes Res.*, vol. 42, no. 5, pp. 942–952, Oct. 2016, doi: 10.1016/j.jglr.2016.07.033.
[26] S. Schulz, S. Darehshouri, E. Hassanzadeh, M. Tajrishy, and C. Schüth, "Climate change or irrigated agriculture—What drives the water level decline of lake Urmia," *Sci. Rep.*, vol. 10, no. 1, Dec. 2020, Art. no. 236, doi: 10.1038/s41598-019-57150-y.
[27] M. R. Zaman, S. Morid, and M. Delavar, "Evaluating climate adaptation strategies on agricultural production in the siminehrud catchment and inflow into lake Urmia, Iran using SWAT within an OECD framework," *Agricultural Syst.*, vol. 147, no. 147, pp. 98–110, 2016.
[28] P. E. O'Neill, S. Chan, E. G. Njoku, T. Jackson, R. Bindlish, and M. J. Chaubell, SMAP Enhanced L3 Radiometer Global Daily 9 km EASE-Grid Soil Moisture, Version 4, NASA National Snow and Ice Data Center Distributed Active Archive Center, Boulder, CO, USA, 2020, doi: 10.5067/NJ34TQ2LFE90.
[29] N. N. Das *et al.*, "SMAP/Sentinel-1 L2 radiometer/radar 30-second scene 3 km EASE-grid soil moisture, version 3, NASA national snow and ice data center distributed active archive center," Boulder, CO, USA, 2020, doi: 10.5067/ASB0EQO2LYJV.
[30] S. K. Chan *et al.*, "Development and assessment of the SMAP enhanced passive soil moisture product," *Remote Sens. Environ.*, vol. 204, pp. 931–941, 2018, doi: 10.1016/j.rse.2017.08.025.
[31] E. Ghafari *et al.*, "On the impact of C-band in place of L-band radar for SMAP downscaling," *Remote Sens. Environ.*, vol. 251, Dec. 2020, Art. no. 112111, doi: 10.1016/j.rse.2020.112111.
[32] M. S. Burgin *et al.*, "A comparative study of the SMAP passive soil moisture product with existing satellite-based soil moisture products," *IEEE Trans. Geosci. Remote Sens.*, vol. 55, no. 5, pp. 2959–2971, May 2017, doi: 10.1109/TGRS.2017.2656859.
[33] N. Das *et al.*, "Algorithm theoretical basis document SMAP-Sentinel L2 radar /Radiometer soil moisture (active/passive) data products: L2 _ SM _ sP," *Jet Propuls. Lab.*, pp. 1–62, 2019.
[34] G. Huffman, E. F. Stocker, D. T. Bolvin, E. J. Nelkin, and T. Jackson, "GPM IMERG final precipitation L3 1 day 0.1 degree x 0.1 degree V06, NASA Goddard Earth Sciences Data and Information Services Center," Boulder, CO, USA, 2019, doi: 10.5067/GPM/IMERGDF/DAY/06.
[35] K. Didan, "MOD13A2 MODIS/Terra vegetation indices 16-day L3 global 1 km SIN grid V006, NASA EOSDIS land processes DAAC," Boulder, CO, USA, 2015, doi: 10.5067/MODIS/MOD13A2.006.

[36] E. G. Njoku and D. Entekhabi, "Passive microwave remote sensing of soil moisture," *J. Hydrol.*, vol. 184, no. 1/2, pp. 101–129, 1996, doi: 10.1016/0022-1694(95)02970-2.
[37] X. Zhang *et al.*, "The potential utility of satellite soil moisture retrievals for detecting irrigation patterns in China," *Water*, vol. 10, no. 11, Oct. 2018, Art. no. 1505, doi: 10.3390/w10111505.
[38] M. Zohaib and M. Choi, "Satellite-based global-scale irrigation water use and its contemporary trends," *Sci. Total Environ.*, vol. 714, Apr. 2020, Art. no. 136719, doi: 10.1016/j.scitotenv.2020.136719.
[39] N. Vergopolan *et al.*, "Combining hyper-resolution land surface modeling with SMAP brightness temperatures to obtain 30-m soil moisture estimates," *Remote Sens. Environ.*, vol. 242, Jun. 2020, Art. no. 111740, doi: 10.1016/j.rse.2020.111740.
[40] J. Zhou, Z. Wu, W. T. Crow, J. Dong, and H. He, "Improving spatial patterns prior to land surface data assimilation via model calibration using SMAP surface soil moisture data," *Water Resour. Res.*, vol. 56, no. 10, Oct. 2020, Art. no. e2020WR027770, doi: 10.1029/2020WR027770.
[41] A. Mousivand *et al.*, "Collaborative crop mapping of the Urmia Lake Basin, Iran, FAO/Urmia Lake Restoration Program (ULRP) joint project," Tehran, Iran, 2020.

Ehsan Jalilvand received the Ph.D. degree in water resources management from the Sharif University of Technology, Tehran, Iran, in 2019.

During his Ph.D., he worked on estimation of precipitation and irrigation using satellite and *in situ* soil moisture data with the Research Institute for Geo-Hydrological protection (CNR-IRPI), Perugia, Italy. In 2019–2020, he started a Postdoctoral Position with the Environmental and Water Research Center, Sharif University of Technology. His research focused on detecting irrigation signals in the high-resolution satellite soil moisture data and assimilation of satellite soil moisture data with land surface models to quantify the irrigation water use. He is currently joining the Biosystem and Agricultural Engineering Faculty, Michigan State University as a Postdoctoral Researcher. He will be involved in the upcoming NASA ISRO SAR (NISAR) mission and primarily work on monitoring changes in the permafrost landscapes and using high-resolution NISAR soil moisture data for agricultural water management at field scale.

Ronnie Abolafia-Rosenzweig received the B.S. degree in civil engineering from Texas A&M University, College Station, TX, USA, in 2016, and the Ph.D. degree in civil engineering from the University of Colorado Boulder, Boulder, CO, USA, in 2020.

During his Ph.D., he worked on land surface modeling and data assimilation with NOAA's Environmental Modeling Center in 2018 and NASA's Land Information System team in 2019–2020. He is currently a Postdoctoral Researcher with the NCAR's Research Applications Laboratory, Boulder, CO, USA. His primary research interests are developing improvements for the Noah-MP land surface model, using remotely sensed soil moisture to better understand irrigation water use, and developing large-scale datasets from remotely sensed observations to quantify the terrestrial water cycle inclusive of human impacts.

Masoud Tajrishy received the B.S. degree in 1988 and the M.S. degree in 1990 in water science and engineering from the University of California at Davis, Davis, CA, USA, and the Ph.D. degree in environmental engineering from the University of California at Davis, Davis, CA, USA, in 1993.

He is currently a Professor with the Department of Civil Engineering, Sharif University of Technology, Tehran, Iran, and he is currently the Science Team Lead for the Urmia Lake Restoration Program that started in 2014. His research interests are remote sensing application in water resources management and agricultural monitoring, wastewater reclamation and reuse, urban run-off modeling, and water quality management.

Narendra N. Das was born in Bhilai, India. He received the B.E. degree in chemical engineering from the National Institute of Technology, Raipur (formerly, Government Engineering College, Raipur), Raipur, India, and the master's and the Ph.D. degrees in biological and agricultural engineering from Texas A&M University, College Station, TX, USA, in 2005 and 2008, respectively.

He is currently an Associate Professor with the Department of Biosystems and Agricultural Engineering, and Department of Civil and Environmental Engineering, Michigan State University (MSU), East Lansing, MI, USA. He joined MSU on November 1, 2020. Prior to joining MSU, he was a Research Scientist with the NASA Jet Propulsion Laboratory (JPL), California Institute of Technology for 12 years (2008–2020). In 2008, he joined JPL, and conducted research in hydrology and microwave remote sensing, especially for soil moisture retrievals using the combination of radiometer and radar, and applications of soil moisture for weather, agriculture, and drought. He is a Science Team member for the Soil Moisture Active and Passive (SMAP) mission.

Dr. Das is the Principal Investigator (PI) of the Applied Science NASA SERVIR program to implement Drought and Crop Forecast System for East Africa region and Lower Mekong Basin Countries. He is a Science Team member of the NASA ISRO SAR (NISAR) mission with the responsibility to produce very high-resolution global soil moisture data product. He is also a PI of NASA Terrestrial Hydrology Program.